Ab initio study of the phase diagram of epitaxial BaTiO$_3$

Oswaldo Diéguez,* Silvia Tinte, A. Antons, Claudia Bungaro, J. B. Neaton,[†] Karin M. Rabe, and David Vanderbilt

Department of Physics and Astronomy, Rutgers University, Piscataway, New Jersey 08854-8019, USA

Using a combination of first-principles and effective-Hamiltonian approaches, we map out the structure of BaTiO$_3$ under epitaxial constraints applicable to growth on perovskite substrates. We obtain a phase diagram in temperature and misfit strain that is qualitatively different from that reported by Pertsev, Zembilgotov, and Tagantsev [Phys. Rev. Lett. **80**, 1988 (1998)], who based their results on an empirical thermodynamic potential with parameters fitted at temperatures in the vicinity of the bulk phase transitions. In particular, we find a region of "*r* phase" at low temperature where Pertsev *et al.* have reported an "*ac* phase." We expect our results to be relevant to thin epitaxial films of BaTiO$_3$ at low temperatures and experimentally achievable strains.

The perovskite oxide barium titanate (BaTiO$_3$) is a proto-typical ferroelectric, an insulating solid whose macroscopic polarization can be reoriented by the application of an electric field.[1] In the perovskite ferroelectrics, it is well known both experimentally and theoretically that the polarization is also strongly coupled to strain,[2] and thus that properties such as the ferroelectric transition temperature and polarization magnitude are quite sensitive to external stress.

Experimentally, the properties of ferroelectrics in thin film form generally differ significantly from those in the bulk.[3] While many factors are expected to contribute to these differences, it has been shown that the properties of perovskite thin films are strongly influenced by the magnitude of the epitaxial strain resulting from lattice matching the film to the substrate. For example, Yoneda *et al.*[4] used molecular-beam epitaxy to grow BaTiO$_3$ (lattice constant of 4.00 Å) on (001)-oriented SrTiO$_3$ (lattice constant of 3.91 Å); they found that the ferroelectric transition temperature exceeds 600 °C, to be compared to the bulk Curie temperature of $T_C = 130$ °C. Other studies have shown that the amount of strain in BaTiO$_3$/SrTiO$_3$ superlattices on SrTiO$_3$ substrates strongly influences properties including the observed polarization, phase transition temperature, and dielectric constant.[5–8]

In a seminal paper, Pertsev, Zembilgotov and Tagantsev[9] introduced the concept of mapping the equilibrium structure of a ferroelectric perovskite material versus temperature and misfit strain, thus producing a "Pertsev phase diagram" (or Pertsev diagram) of the observable epitaxial phases. The effect of epitaxial strain is isolated from other aspects of thin-film geometry by computing the structure of the *bulk* material with homogeneous strain tensor constrained to match a given substrate with square surface symmetry.[10] In addition, short-circuit electrical boundary conditions are imposed, equivalent to ideal electrodes above and beneath the film.[9] Given the recognized importance of strain in determining the properties of thin-film ferroelectrics, Pertsev diagrams have proven to be of enormous interest to experimentalists seeking to interpret the results of experiments on epitaxial thin films and heterostructures.

In Ref. 9 the mapping was carried out with a phenomeno-logical Landau–Devonshire model taken from the literature.

This should give excellent results in the temperature/strain regime in which the model parameters were fitted, but will generally be less accurate when extrapolated to other regimes. In Fig. 1, we compare two Pertsev diagrams for BaTiO$_3$ computed using two different sets of Landau–Devonshire parameters, used by Pertsev and co-workers in Refs. 9 and 11, respectively. While both give the same behavior near the bulk T_C and small misfit strains, they predict completely different low-temperature phase behavior.

With first-principles methods, it is possible not only to resolve such discrepancies arising in phemenogical theories, but also to generate a wealth of microscopic information about the structure and properties of epitaxial phases at various temperatures and substrate lattice constants. In this paper, using parameter-free total-energy methods based on density functional theory (DFT), we map out the equilibrium structure of BaTiO$_3$ as a function of epitaxial constraints at zero temperature, and then extend the results to finite temperature via an effective-Hamiltonian approach. The Pertsev diagram obtained in this way has a similar global topology as that of Ref. 11 (but not to the one in Ref. 9). This allows us to predict the impact of misfit strain on the magnitude and
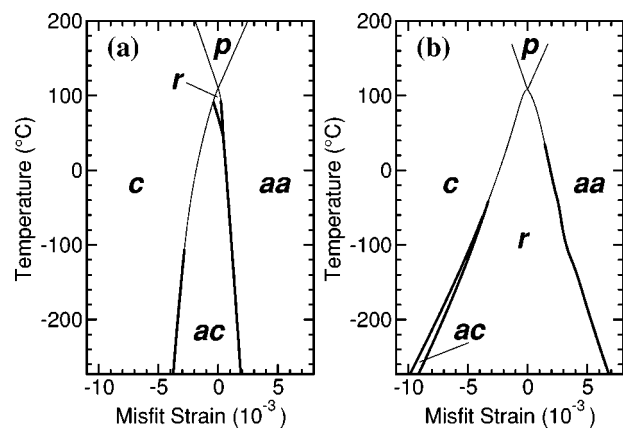

FIG. 1. Phase diagrams of epitaxial BaTiO$_3$ as predicted by the theory of Pertsev *et al.* (see Ref. 9). (a) Using the parameters quoted in Ref. 9. (b) Using the parameters quoted in Ref. 11. The second- and first-order phase transitions are represented by thin and thick lines, respectively.

TABLE I. Summary of possible epitaxial BaTiO$_3$ phases. In-plane cell vectors are fixed at $\mathbf{a}_1 = a\hat{x}$, $\mathbf{a}_2 = a\hat{y}$. Columns list, respectively: phase; space group; out-of-plane lattice vector; number of free internal displacement coordinates; and form of the polarization vector.

Phase	SG	$\mathbf{a}_3$	N_p	Polarization
p	$P4mmm$	$c\hat{z}$	0	0
c	$P4mm$	$c\hat{z}$	3	$P_z\hat{z}$
aa	$Amm2$	$c\hat{z}$	4	$P(\hat{x}+\hat{y})$
a	$Pmm2$	$c\hat{z}$	4	$P\hat{x}$
ac	Pm	$c_\alpha\hat{x}+c\hat{z}$	8	$P\hat{x}+P_z\hat{z}$
r	Cm	$c_\alpha(\hat{x}+\hat{y})+c\hat{z}$	7	$P(\hat{x}+\hat{y})+P_z\hat{z}$

orientation of the polarization and Curie temperature of BaTiO$_3$. Our results should thus be of considerable importance for understanding experimental growth of high-quality, coherent epitaxial thin films of BaTiO$_3$ on perovskite substrates, as well as more generally illustrating the utility of first-principles Pertsev diagrams.

The first-principles DFT calculations are carried out in the Kohn–Sham framework[12] using the VASP software package.[13] The electron-ion interaction is described by the projector augmented wave method;[14] semicore electrons are included in the case of Ba ($5s^25p^66s^2$) and Ti ($3s^23p^64s^23d^2$). The calculations employ the Ceperley–Alder[15] form of the local-density approximation (LDA) exchange-correlation functional,[16] a 700 eV plane-wave cutoff, and a $6\times6\times6$ Monkhorst–Pack sampling of the Brillouin zone.[17]

We begin by systematically performing optimizations of the five-atom unit cell of the cubic perovskite structure (space group $Pm\bar{3}m$) in the six possible phases considered by Pertsev and co-workers in Ref. 9. A description of these phases is given in Table I. Starting from a structure in which the symmetry is established by displacing the Ti and O atoms, we relax the atomic positions and the out-of-plane cell vector until the value of the Hellmann–Feynman forces and zz, yz and zx stress tensor components fall below some given thresholds (0.001 eV/Å and 0.005 eV, respectively).

In Fig. 2 we present the computed energy for each phase as a function of the misfit strain $s = a/a_0 - 1$, where a_0 is our DFT lattice constant for free cubic BaTiO$_3$ (3.955 Å). For large compressive strains, the lowest energy corresponds to the c phase; for large tensile strains, the aa phase is favored. At a misfit strain of $s_{\max}(c) = -6.4\times10^{-3}$ ($a = 3.930$ Å), there is a second-order transition from the c phase to the r phase, with the polarization in the r phase continuously rotating away from the z direction as the misfit strain increases. At misfit strain $s_{\min}(aa) = 6.5\times10^{-3}$ ($a = 3.981$ Å), the r phase polarization completes its rotation into the xy plane, resulting in a continuous transition to the aa phase. The minimum energy r phase is at misfit strain of 2.2×10^{-3} ($a = 3.964$ Å); lattice matching to the substrate would be optimal at this point. At the misfit strain of the $c\rightarrow r$ transition, the polarization could also begin a continuous rotation into the (010) plane, corresponding to the ac phase. However, it is clear from the figure that the energy of the ac phase is always
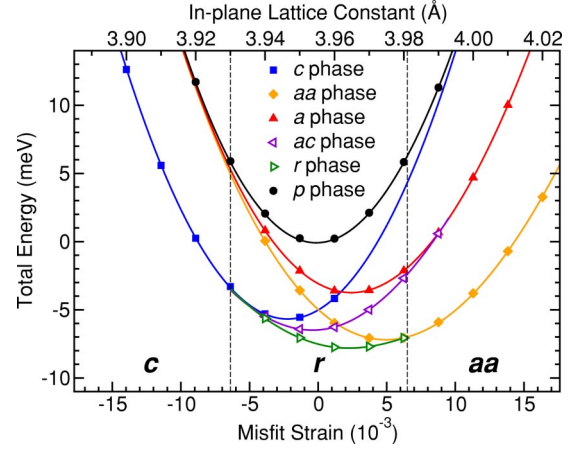

FIG. 2. (Color online) Energies of the possible epitaxial BaTiO$_3$ phases for different misfit strains, as obtained from the full *ab initio* calculations. The vertical lines denote the phase transition points given by the stability analysis.

higher than that of the r phase, which makes sense given that the r phase is an epitaxial distortion of the ground-state rhombohedral phase of bulk BaTiO$_3$, while the ac phase is related to the higher-energy bulk orthorhombic phase. We conclude that the phase sequence at low temperatures is not $c\rightarrow ac \rightarrow aa$ as given in Ref. 9, but $c\rightarrow r\rightarrow aa$.

Figure 3 shows the computed behavior of the atomic displacements for the lowest-energy phase with increasing misfit strain. For large compressive strains, the pattern of displacements corresponds to the c phase, and atoms relax only along the [001] direction. As the in-plane strain increases, we observe a second-order phase transition ($c\rightarrow r$), and while the magnitude of the atomic displacements continues to diminish along [001], the displacements in the xy plane begin to grow. With increasing tensile strain, the displacements along [001] vanish at the $r\rightarrow aa$ transition, while the dis-
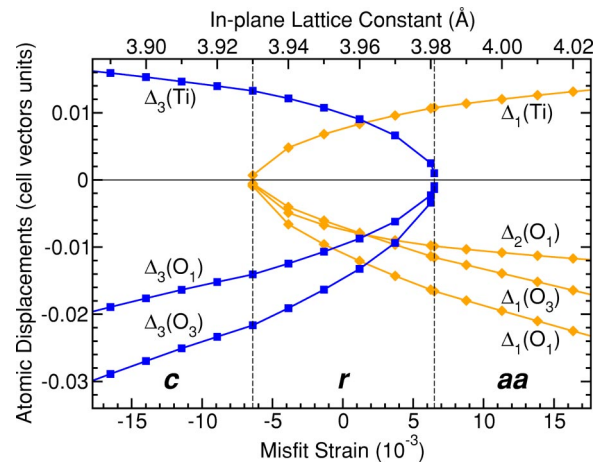

FIG. 3. (Color online). Displacements of the atoms from the cubic perovskite cell positions, for the most energetically favorable configuration at a given misfit strain. The vertical lines denote the phase transition points obtained from the stability analysis. Δ_3(Ti) labels the displacement of the Ti atom in units the third lattice vector, etc.

placements in the xy plane continue to grow smoothly. Similar results are found when we analyze the $c \rightarrow ac \rightarrow a$ sequence (not shown), where what was said for the xy plane applies now to the [100] direction. The clear change in character of the displacement pattern within the r phase witnessed here illustrates the quantitative limitations of using a single misfit-strain-independent local mode to model the phase diagram.

A stability analysis provides the precise limits of phase stability shown in Figs. 2 and 3. At each value of misfit in the c phase, for example, we carry out finite-difference calculations of x forces and xz stress as the atomic x coordinates and xz strain are varied. The zero crossing of the lowest eigenvalue of the resulting 6×6 Hessian matrix identifies the critical misfit. A similar analysis is used to consider z displacements and shear strains in the a and aa phases. By properly considering zone-center phonons, elastic shear, and linear cross coupling between them, this analysis allows us to locate the second-order phase boundaries much more precisely than is possible through direct comparison of total energies.[18]

Having established the first principles zero-temperature phase diagram, we now extend our study of epitaxial BaTiO$_3$ to finite temperatures using the effective Hamiltonian approach of Zhong, Vanderbilt, and Rabe.[19] In this method, the full Hamiltonian is mapped onto a statistical mechanical model by a subspace projection, and parametrized through *ab initio* calculations of small distortions of bulk BaTiO$_3$ in the cubic perovskite structure. The reduced subspace is composed of a set of relevant degrees of freedom identified for ferroelectric perovskites as the unit cell distortions corresponding to local polarization, expressed in the form of local modes. This subspace is augmented by the inclusion of the homogeneous strain.

It is straightforward to impose the constraint of fixed in-plane strain by fixing three of the six tensor strain components during the Monte Carlo (MC) simulations. For each value of in-plane strain, MC thermal averages are obtained for the unconstrained components of the homogeneous strain and the average polarization,[20] and phase transitions are identified by monitoring the symmetry of these quantities. Following Ref. 19, all the simulations were performed at the same negative external pressure of $P = -4.8$ GPa. Misfit is defined relative to $a_0 = 3.998$ Å, the lattice constant at the bulk cubic-to-tetragonal transition as computed with this approach.[19] The resulting phase diagram appears in Fig. 4, where all phase lines represent second-order transitions.

The Pertsev diagrams of Figs. 1(a), 1(b), and 4 share the same topology above and just below T_C: p at high temperature, c at large compressive misfit, aa at large tensile misfit, and a four-phase point connecting these phases with the r phase at T_C. At lower temperature, there is a drastic difference between Figs. 1(a) and 1(b), with our theory supporting the latter. While our theory underestimates the temperature of the four-phase crossing point in Fig. 4 by about 100 °C, this is the price we pay for insisting on a first-principles approach; indeed, this effective Hamiltonian underestimates the temperature of the bulk cubic-to-tetragonal transition by about the same amount.

At low temperature, our Pertsev diagram shows the sequence of second-order phase transitions $c \rightarrow r \rightarrow aa$. The r
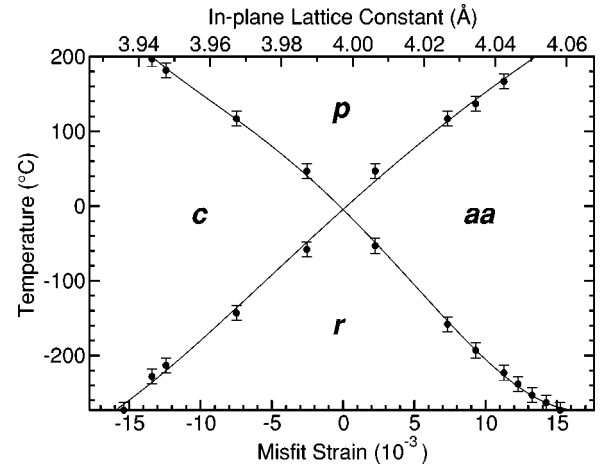

FIG. 4. Phase diagram of epitaxial BaTiO$_3$ obtained using the effective Hamiltonian of Zhong, Vanderbilt and Rabe (see Ref. 19).

phase is predicted to exist in a range that is more than twice as broad as that shown in Fig. 2. We have found that this range is reduced to about 1.5 times that of Fig. 2 when the negative-pressure correction is not included. The remaining discrepancy is related to technical differences between the DFT calculations used in Ref. 21 to obtain the parameters for the effective Hamiltonian method and the DFT calculations we report here.[22] We should also mention that the effective Hamiltonian used does not include the physics related to the zero-point motion of the ions. This quantum effect should alter the shape of the lines of the diagram at very low temperatures, and it would result in those lines approaching the misfit-strain axis with infinite derivative (see, for example, Ref. 23). In any case, at zero temperature, the phase sequence is quite unambiguously established by the first-principles results. This clearly indicates that the low-temperature extrapolation of the Landau–Devonshire parameters fitted near T_C can give rise to spurious results, such as the stability of the ac phase obtained in Ref. 9.

Finally, we comment on the effect of the assumptions made in the construction of this first-principles Pertsev diagram. In principle, we should consider the possibility of equilibrium structures with larger unit cells, particularly those with cell-doubling octahedral rotations, which have been shown to be important in SrTiO$_3$, and could condense in BaTiO$_3$ under sufficiently large misfit strains. As an example, we have checked that the paraelectric phase of the film is stable with respect to octahedral rotations about the [001] direction (with M_3 symmetry) up to an epitaxial compressive strain of -70.9×10^{-3} ($a = 3.675$ Å), far larger than those likely to be experimentally relevant. In addition, while we have studied only the effects of epitaxial strain, other physical effects may also be relevant to the structure and properties of thin films, such as atomic rearrangements at the film-substrate interface and free surface, and the instability to formation of multiple domain structures.[24]

To summarize, we have performed density functional theory calculations in order to obtain the Pertsev diagram of epitaxial BaTiO$_3$ at zero temperature. The results we obtain differ from those computed previously[9] using a Landau–Devonshire theory where the parameters needed were ob-

tained from experimental information about bulk $BaTiO_3$ at the phase transitions temperatures. Alternatively, the use of a similar theory where the constants of the model are computed using an *ab initio* method is consistent with both the first principles results at zero temperature, and with the work of Pertsev and co-workers[9] at high temperature.

*Electronic address: dieguez@physics.rutgers.edu

†Present address: The Molecular Foundry, Materials Sciences Division, Lawrence Berkeley National Laboratory, Berkeley, CA 94720.

[1] M. E. Lines and A. M. Glass, *Principles and Applications of Ferroelectrics and Related Materials* (Clarendon, Oxford, 1977).

[2] R. E. Cohen, Nature (London) **358**, 136 (1992).

[3] C. H. Ahn, K. M. Rabe, and J.-M. Triscone, Science **303**, 488 (2004).

[4] Y. Yoneda, T. Okabe, K. Sakaue, H. Terauchi, H. Kasatani, and K. Deguchi, J. Appl. Phys. **83**, 2458 (1998).

[5] W. Chang, C. M. Gilmore, W.-J. Kim, J. M. Pond, S. W. Kirchoefer, S. B. Qadri, D. B. Chrisey, and J. S. Horwitz, J. Appl. Phys. **87**, 3044 (2000).

[6] H. Li, A. L. Roytburd, S. P. Alpay, T. D. Tran, L. Salamanca-Riba, and R. Ramesh, Appl. Phys. Lett. **78**, 2354 (2001).

[7] T. Shimuta, O. Nakagawara, T. Makino, S. Arai, H. Tabata, and T. Kawai, J. Appl. Phys. **91**, 2290 (2002).

[8] J. B. Neaton and K. M. Rabe, Appl. Phys. Lett. **82**, 1586 (2003).

[9] N. A. Pertsev, A. G. Zembilgotov, and A. K. Tagantsev, Phys. Rev. Lett. **80**, 1988 (1998).

[10] The applicability of our study is thus not limited to cubic substrates; it also applies, e.g., to tetragonal perovskite substrates.

[11] N. A. Pertsev, A. G. Zembilgotov, and A. K. Tagantsev, Ferroelectrics **223**, 79 (1999).

[12] P. Hohenberg and W. Kohn, Phys. Rev. **136**, B864 (1964); W. Kohn and L. J. Sham, *ibid.* **140**, A1133 (1965).

[13] G. Kresse and J. Hafner, Phys. Rev. B **47**, 558 (1993); G. Kresse and J. Furthmüller, *ibid.* **54**, 11169 (1996).

[14] P. E. Blöchl, Phys. Rev. B **50**, 17953 (1994); G. Kresse and D. Joubert, *ibid.* **59**, 1758 (1999).

[15] D. M. Ceperley and B. J. Alder, Phys. Rev. Lett. **45**, 566 (1980).

[16] Using the generalized gradient approximation instead of the LDA does not lead to substantial improvements in the case of $BaTiO_3$; see D. J. Singh, Ferroelectrics **164**, 143 (1995).

[17] H. J. Monkhorst and J. D. Pack, Phys. Rev. B **13**, 5188 (1976).

[18] Similarly, the a phase is stable against the ac phase down to $s_{min}(a) = 10.3 \times 10^{-3}$ ($a = 3.993$ Å). Omitting the strain and working only with the 5×5 Hessian matrix results in very little error: $s_{max}(c) = -6.2 \times 10^{-3}$ ($a = 3.931$ Å), $s_{min}(aa) = 6.1 \times 10^{-3}$ ($a = 3.980$ Å), and $s_{min}(a) = 9.3 \times 10^{-3}$ ($a = 3.992$ Å).

[19] W. Zhong, D. Vanderbilt, and K. M. Rabe, Phys. Rev. Lett. **73**, 1861 (1994); Phys. Rev. B **52**, 6301 (1995).

[20] MC simulations were performed using a $12 \times 12 \times 12$ supercell. Typically 30 000 MC sweeps were used to equilibrate the system, and an additional 50 000 to obtain averages of local-modes variables with a statistical error below 10%. The temperature was increased in steps of 5 K.

[21] R. D. King-Smith and D. Vanderbilt, Phys. Rev. B **49**, 5828 (1994).

[22] In particular, the soft-mode eigenvalue has been found to be very sensitive to the fineness of the grid used to evaluate the Fourier transforms. This discrepancy vanishes almost completely if instead of working with the soft-mode eigenvalue calculated in Ref. 21 (0.0350 a.u.) we use the one given by our new DFT calculations (0.0223 a.u.), that was calculated using a finer grid.

[23] J. Íñiguez and D. Vanderbilt, Phys. Rev. Lett. **89**, 115503 (2002).

[24] Y. L. Li, S. Choudhury, Z. K. Liu, and L. Q. Chen, Appl. Phys. Lett. **83**, 1608 (2003).